



Article

Cu(II)–N⁶-Alkyladenine Complexes: Synthesis, X-ray Characterization and Magnetic Properties

María Soledad Martínez ¹, Antonio Bauzá ¹, Amparo Caubet ², Ángel García-Raso ¹,
Ángel Terrón ¹, Juan J. Fiol ¹, Elies Molins ³ , Miquel Barceló-Oliver ¹
and Antonio Frontera ^{1,*} 

¹ Departament de Química, Universitat de les Illes Balears, Ctra. de Valldemossa km 7.5, 07122 Palma de Mallorca, Balears, Spain; marisol.martinez.riutort@hotmail.com (M.S.M.); antonio.bauza@uib.es (A.B.); angel.garcia-raso@uib.es (Á.G.R.); angel.terron@uib.es (Á.T.); jfa950@uib.es (J.J.F.); miquel.barcelo@uib.es (M.B.-O.)

² Department of Inorganic and Organic Chemistry, University of Barcelona, Martí i Franquès 1-11, 08028 Barcelona, Spain; amparo.caubet@qi.ub.es

³ Institut de Ciència de Materials de Barcelona (ICMAB-CSIC), Campus Universitat Autònoma de Barcelona, 08193 Cerdanyola, Spain; elies.molins@icmab.es

* Correspondence: toni.frontera@uib.es; Tel.: +34-971-173-498

Received: 8 May 2018; Accepted: 19 May 2018; Published: 23 May 2018



Abstract: Three new dinuclear copper(II) complexes [Cu₂(μ-HLⁿ)₂(μ-Cl)₂Cl₂]Cl₂ (**1–3**) have been synthesized and structurally characterized by single-crystal X-ray diffraction, where HL^x, (HL¹ = N⁶-propyladeninium, HL² = N⁶-butyladeninium and HL³ = N⁶-isobutyladeninium) are N⁶-alkyl bidentate NN donor adenine bases. Complexes **1–3** exhibit a coplanar arrangement of both N⁶-alkyladeninium moieties with UD conformation, with the terms U(up) or D(down) referring to the coordination of each pyrimidinic N³ atoms to the upper or lower metal center. In the three complexes, both copper atoms are five-coordinated (N₂Cl₃ donor set), resembling a compressed trigonal bipyramid. Each adenine moiety is protonated in N¹ and the positive charge balanced by chloride counterions. Magnetic measurements of complexes **1** and **3** in the 2–300 K temperature range indicate antiferromagnetic coupling with $J = -156.1(7)$ and $J = -151(2)$ cm⁻¹, respectively. Density functional theory calculations have also been performed in order to estimate the exchange coupling constants in these complexes. The theoretically calculated J values are in good agreement with the experimental values.

Keywords: Cu(II) complexes; N⁶-alkyladenine ligand; antiferromagnetic coupling; DFT calculations

1. Introduction

The chemistry of transition metal coordination to purine nucleobases has been extensively studied, paying special attention to its structural diversity, biological importance and molecular recognition [1,2]. Moreover, coordination compounds involving nucleobases have interesting potential applications as advanced functional materials [3–5]. In particular, adenine (6-aminopurine) presents many binding possibilities using the endocyclic N¹, N³, N⁷, N⁹ or exocyclic N⁶ atoms as coordination sites [6,7], giving rise to a great number of possibilities. Furthermore, upon the formation of the metal–adenine complex, the remaining non-coordinated N-atoms' donor sites are good hydrogen bond acceptors, thus conferring the ability to form supramolecular assemblies [8,9].

The ability of purine ligands to form dinuclear complexes via the N³ and N⁹ bridging mode is well known [10–13]. Moreover, previous research has shown that adenine and adeninate ligands have a marked tendency to form paddle-wheel shaped dinuclear Cu(II) complexes [14–17]. In this

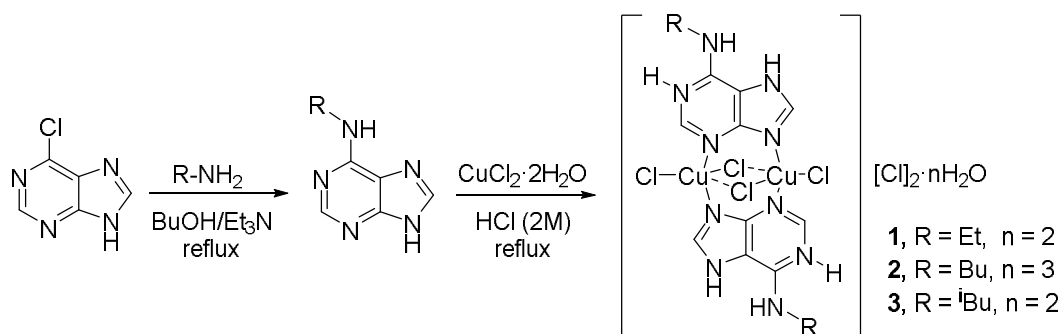
regard, Castillo and co-workers have synthesized paddle-wheel-shaped complexes of formulae $[\text{Cu}_2(\mu\text{-adenine})_4]^{4+}$, $[\text{Cu}_2(\mu\text{-adeninato})_4]$, or $[\text{Cu}_2(\mu\text{-adeninato})_2(\text{X})_2]$ ($\text{X} = \text{Cl}, \text{Br}, \text{NO}_3^-$) [18] and studied their ability to form supramolecular assemblies and supramolecular metal organic frameworks (SMOFs) in the solid state governed by the formation of H-bonding and π - π stacking interactions [19]. Moreover, it has been previously described in the literature that halide- and pseudohalide-bridged bimetallic copper(II) complexes exhibit from moderate to strong antiferromagnetic superexchange interactions [20–22].

To the best of our knowledge, the solid state structure of dinuclear Cu(II) complexes through the N^3 and N^9 bridging mode using N^1 -protonated adenine nucleobase is not available in the literature. In this manuscript we report the synthesis and X-ray characterization of three new dinuclear copper(II) complexes, $[\text{Cu}(\mu\text{-HL}^1)_2(\mu\text{-Cl})_2\text{Cl}_2]\text{Cl}_2$ (**1**), $[\text{Cu}(\mu\text{-HL}^2)_2(\mu\text{-Cl})_2\text{Cl}_2]\text{Cl}_2$ (**2**) and $[\text{Cu}(\mu\text{-HL}^3)_2(\mu\text{-Cl})_2\text{Cl}_2]\text{Cl}_2$ (**3**), where HL^1 , HL^2 , and HL^3 are N^6 -propyladeninium, N^6 -butyladeninium, and $\text{HL}^3 = \text{N}^6$ -isobutyladeninium, respectively. Complexes **1–3** exhibit a coplanar arrangement of both N^6 -alkyladeninium moieties and both copper atoms are five-coordinated (N_2Cl_3 donor set). Variable temperature magnetic susceptibility experiments of complexes **1** and **3** show antiferromagnetic interactions between the Cu(II) centers. Density functional theory (DFT) calculations have been carried out to confirm the exchange coupling constants in these complexes and rationalize the super-exchange mechanism.

2. Results and Discussion

2.1. Synthesis

The N^6 -adenine derivatives were prepared by the 1:1 condensation of 6-chloropurine with the corresponding amine (ethylamine, butylamine or isobutylamine) in *n*-butanol/triethylamine following the literature method (see Scheme 1). For the synthesis of the complexes, $\text{CuCl}_2 \cdot 2\text{H}_2\text{O}$ and HL^n in a 2:1 molar ratio in HCl 2M, were reacted under reflux for 4 h, yielding, by slow evaporation of the solution over several weeks, the corresponding complex in a moderate yield (40–55%).



Scheme 1. Synthetic route to complexes **1–3**.

2.2. IR Spectra of the Complexes

All three complexes show two broad bands, one around 3400 cm^{-1} due to the presence of water and the other around 3300 cm^{-1} due to the presence of the exocyclic N–H group in adenine, as reported in the literature [23,24]. Typical bands of the N^1 -protonated adenine ring are observed at $1697\text{--}1698\text{ cm}^{-1}$ in the IR spectra of all three complexes, which are found approximately at a 30 cm^{-1} higher wave number than usual due to the coordination of adenine to the Cu atoms.

2.3. Structural Description of the Structures

All compounds consist of dicationic dimeric $[\text{Cu}_2(\mu\text{-N}^6\text{-alkyladeninium})_2(\mu\text{-Cl})_2(\text{Cl})_2]^{2+}$ entities (Figure 1). They are similar to the previously described $[\text{Cu}_2(\mu\text{-N}^6\text{-alkyladenine})_2(\mu\text{-X})_2(\text{X})_2]$ ($\text{X} = \text{Cl}, \text{Br}$)

neutral dimeric complexes [25]. The adenine moiety is protonated in N1 and the chloride counterions are coplanar to the adenine rings, interacting with N6–H and N3–H groups to establish bifurcated H-bonds. Curiously, the counterions do not interact with the protonated N1⁺–H group because it is interacting with the water molecules, as further described below (see Figure 2). The complexes show the typical UD conformation [referring the terms U(up) or D(down) to the coordination of each pyrimidinic N³ atoms to the upper or lower metal center with regard to the adeninium bridges and two capping chloride anions]. The intradimeric Cu...Cu distances are 2.962(2), 2.967(2) and 2.953(2) Å and each copper atom is pentacoordinated by a N₂Cl₃ donor set. The coordination distances and angles are given in Table S1 (see ESI or Supplementary Materials), the Cl–Cu–Cl angles range from 94 to 161° and the N3–Cu–N9 angle is in the range 162–166°. The Cu–Cl distances of the bridging chloride anions are slightly longer than those of the terminal one, as is common in this type of complex [25]. Finally, the Cu–N3 distance is longer than that of Cu–N(9), which indicates the stronger *s*-character of the lone pair (LP) orbital used in the coordination by N9 [25].

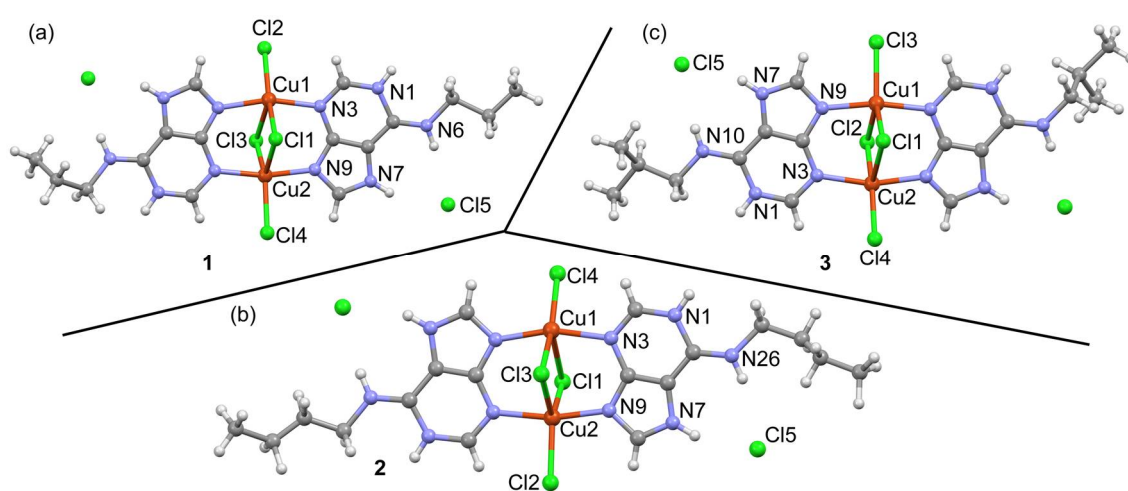


Figure 1. X-ray structure of complexes **1** (a), **2** (b) and **3** (c), with indication of the atom numbering scheme. For compounds **1** and **3**, the alkyl chains present disorder and only one position is given.

The solid state structure of these complexes is governed by the formation of a hydrogen bonding network due to an intricate combination of strong hydrogen bonds (N–H...O, N–H...Cl and O–H...Cl) generating 2D sheets (see Figure 2 for complex **3** as a representative model, see ESI for the same representation of compounds **1** and **2**). The geometrical features of the hydrogen bonds are given in Table 1. The Cl6 is engaged in a bifurcated H-bond with the exocyclic N–H and N7–H groups and also with the water molecule that connects two [Cu₂(μ-N⁶-alkyladeninium)₂(μ-Cl)₂(Cl)₂]²⁺ entities via the N1–H bond. The geometric characteristics of the hydrogen bonding interactions are summarized in Table 1 for compound **3** and Tables S2 and S3 (ESI) for compounds **1** and **2**, respectively.

The final 3D structure is given in Figure 3 and is formed by the interaction of the layers by means of additional H-bonding interactions that are formed between the chloride anions and water molecules.

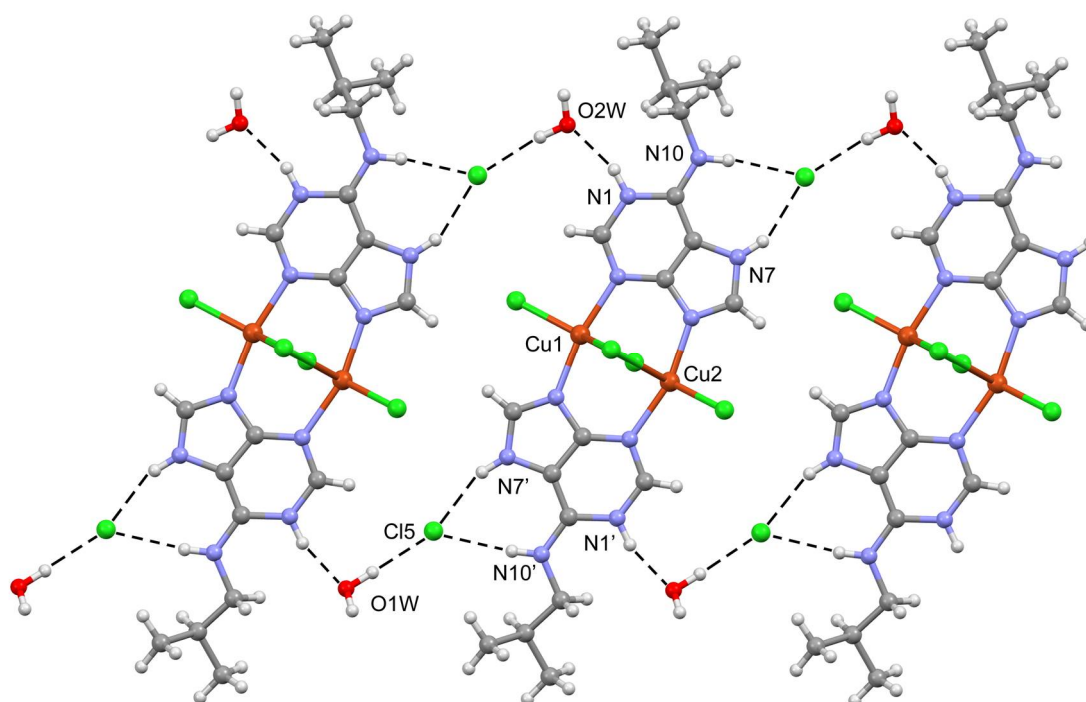


Figure 2. H-bonding network forming 2D supramolecular structures in compound 3. See footnote of Table 1 for symmetry operations of N1', N7', and N10'.

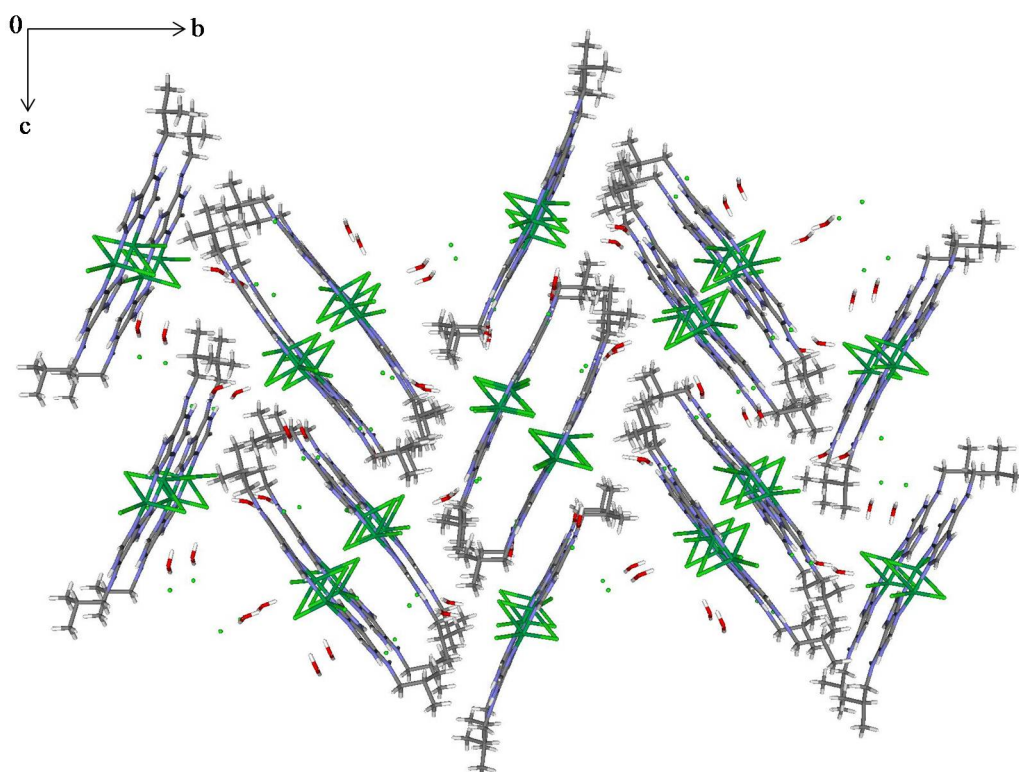


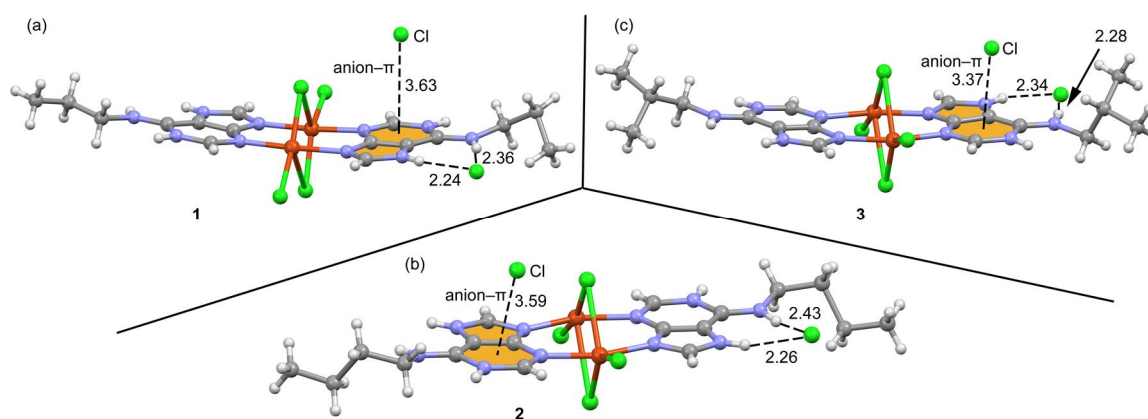
Figure 3. Crystal packing of compound 3 (*bc* plane).

Table 1. Geometric features of the hydrogen bonds in compound **3**. Distances in Å and angles in degrees.

D-H...A ¹	d(H...A)	d(D...A)	<(DHA)
N(1)-H(1)...O(1W) # ¹	1.83	2.671(15)	165.2
N(1')-H(1')...O(2W) # ³	1.88	2.707(13)	160.3
N(7)-H(7)...Cl(5) # ²	2.31	3.132(11)	159.0
N(7')-H(7')...Cl(6) # ⁴	2.24	3.045(11)	156.7
N(10)-H(10)...Cl(5) # ²	2.34	3.196(12)	172.0
N(10')-H(10')...Cl(6) # ⁴	2.36	3.210(12)	168.0
O(1W)-H(1W2)...Cl(5)	2.32(15)	3.078(13)	141(20)
O(2W)-H(2W2)...N(3') # ⁵	2.84(12)	3.258(14)	110(9)
O(2W)-H(2W1)...N(1') # ⁵	2.99(17)	3.476(16)	116(14)
O(1W)-H(1W1)...Cl(2)	2.34(4)	3.208(12)	161(9)
O(2W)-H(2W2)...Cl(3) # ⁵	2.35(3)	3.238(11)	173(12)

¹ Symmetry operations: #¹: $-x+1, -y+1, -z+1$; #²: $-x+2, -y+1, -z+1$; #³: $x+1, y-1, z$; #⁴: $x, y-1, z$; #⁵: $-x+1, -y+1, -z$.

It is worth mentioning that, in all solid state crystal structures, the 2D layers are also interconnected by the formation of anion- π interactions. A detailed description of this interaction, which involves the chloride anion and the six-membered ring of the adenine, is shown in Figure 4. The anion- π distances observed for **1-3** are similar to those previously reported for adenine derivatives and several anions like nitrate [26], chloride [27], HgCl_4^{2-} , and ZnCl_4^{2-} [28].

**Figure 4.** Detail of the anion- π interactions observed in compounds **1** (a), **2** (b) and **3** (c). Distances in Å.

2.4. Magnetic Study

The temperature dependence of the molar magnetic susceptibility, χ_M , of compounds **1** and **3** was measured under a magnetic field of 1 T over the temperature range 300–2 K. Figure 5 (top) shows the plots of $\chi_M T$ versus temperature, T , for compounds **1** and **3**. At 300 K, the values of $\chi_M T$ are 0.73 (**1**) and 0.77 $\text{cm}^3 \text{mol}^{-1} \text{K}$ (**3**), which are consistent with the expected values for two Cu(II) ions (0.75 $\text{cm}^3 \text{mol}^{-1} \text{K}$, for $g = 2.0$). The χ_M values for **1** (**3**) increase on cooling from $2.4 \times 10^{-3} \text{cm}^3 \text{mol}^{-1}$ ($2.6 \times 10^{-3} \text{cm}^3 \text{mol}^{-1}$) at 300 K to a maximum of $3.3 \times 10^{-3} \text{cm}^3 \text{mol}^{-1}$ ($3.6 \times 10^{-3} \text{cm}^3 \text{mol}^{-1}$) at 125 K. After, the χ_M values for **1** and **3** decrease to a minimum of $5.9 \times 10^{-4} \text{cm}^3 \text{mol}^{-1}$ ($1.4 \times 10^{-3} \text{cm}^3 \text{mol}^{-1}$) at 33 K and increase to a value of $1.7 \times 10^{-3} \text{cm}^3 \text{mol}^{-1}$ ($9.5 \times 10^{-3} \text{cm}^3 \text{mol}^{-1}$) at 2 K due to paramagnetic impurities (see Figure 5, bottom). The magnetic behavior of **1** and **3** indicates strong antiferromagnetic coupling.

The experimental magnetic data have been fitted using the Bleaney-Bowers expression based on the Hamiltonian $H = -JS_A S_B$ with $S_A = S_B = \frac{1}{2}$ (Equation (1))

$$\chi_M = ((2Ng^2\mu_B^2/kT)(3 + \exp(-J/kT))^{-1})(1 - \rho) + (Ng^2\mu_B^2/4kT)\rho + N\alpha \quad (1)$$

The parameters N , μ_B and k in Equation (1) have their usual meanings, J = singlet-triplet splitting, ρ = molar fraction of non-coupled species and $N\alpha$ (T.I.P.) = $60 \times 10^{-6} \text{ cm}^3 \text{ mol}^{-1}$. The g -values (2.18 and 2.16 for **1** and **3**, respectively) can be estimated from the EPR spectra (see below). Least-square fitting of all experimental data leads to the following parameter $J = -156.1$ (7) cm^{-1} and $\rho = 0.019$ for **1** and $J = -151.0$ (2) cm^{-1} and $\rho = 0.044$ for **3**.

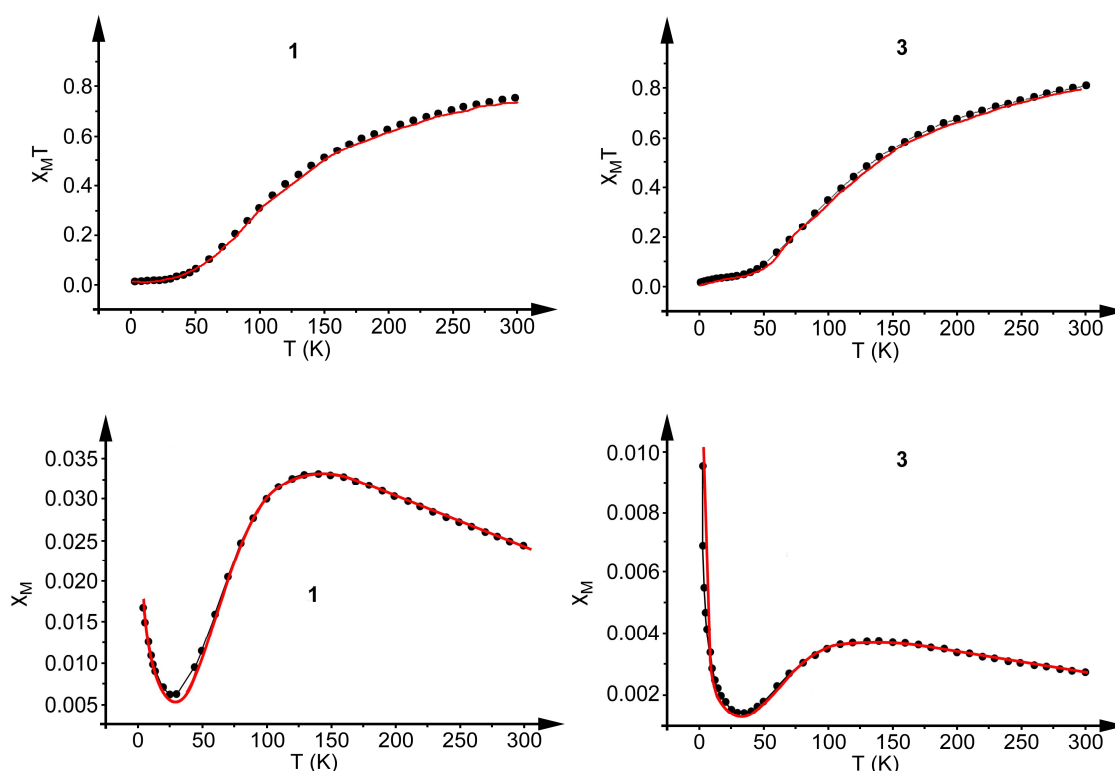


Figure 5. (Top) Temperature dependence of χ_{MT} ($\text{cm}^3 \text{ mol}^{-1} \text{ K}$) of a solid sample of compounds **1** and **3**. (Bottom) Temperature dependence of χ_M ($\text{cm}^3 \text{ mol}^{-1}$) of a solid sample of compounds **1** and **3**. The solid red lines represent the best fit. $R = \sum(\chi_{MT}^{\text{calc}} - \chi_{MT}^{\text{obs}})^2 / \sum(\chi_{MT}^{\text{obs}})^2$ inferior to 1.0×10^{-4} .

2.5. EPR Spectra

The X-band EPR spectra of compounds **1** and **3** measured at 298 K are shown in Figure S3 showing in both cases a single and symmetric strong band with $g_{\text{iso}} = 2.18$ and 2.16 for **1** and **3**, respectively. These experimental g values have been used to obtain the J values commented above. The X-band EPR spectrum for a polycrystalline sample of **3** in the temperature range 4 K–298 K is shown in Figure 6. At 4 K one symmetric transition was observed at 3142 G without any hyperfine features (blue line). The intensity of this signal is temperature-dependent, showing an initial rise at 30 K (red line) that further increases and broadens at 77 K (green line). Finally, it becomes less intense at 298 K (black line). This initial increase and subsequent decrease of signal intensity with rise in temperature is consistent with the presence of antiferromagnetic coupling interactions within the copper centers. The lack of fine structures in the spectra at low temperatures (<77 K) is consistent with the presence of intercluster exchange interactions that tend to average out the fine structures arising from the multiplets.

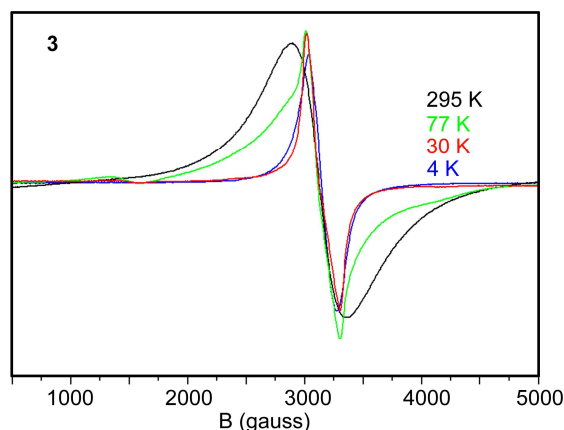


Figure 6. X-band EPR spectra at 4 K to 295 K for a microcrystalline sample of **3**.

2.6. Theoretical Study

We therefore used UB3LYP/6-31+G* calculations (broken symmetry approach, see theoretical methods) to evaluate the magnetic coupling constant J in **1** and **3**. The theoretical value of J values computed at this level of theory (-109.3 and -112.5 cm^{-1} for **1** and **3**, respectively) are in reasonable agreement with the experimental ones (-151 cm^{-1}) and confirms the anti-ferromagnetic coupling in both compounds. To investigate the mechanism for the magnetic exchange coupling, the spin density distribution was analyzed in compound **3** as a representative compound. The atomic spin population values on the Cu metal centers and the donor atoms of the ligands are listed in Table 2. The absolute energies and $\langle S^2 \rangle$ values are given in the ESI (see Table S4).

Table 2. Atomic spin densities (e) computed for the high and low spin configuration of **3** at the B3LYP/6-31+G* level of theory.

Atom Label	High Spin	Low Spin
Cu1	0.56	-0.57
Cu2	0.59	0.57
Cl1	0.14	-0.12
Cl2	0.14	0.13
Cl3	0.17	-0.17
Cl4	0.14	0.15
N3/N3'	0.05	0.05/-0.05
N9/N9'	0.07	0.07/-0.07
C4/C4'	0.01	0.00

For the high-spin (HS) configuration, the Mulliken spin population data shows that significant spin (ca. 0.85 e) is delocalized through the ligands, and the rest (1.15 e) is supported by the Cu ions. The spin density plots corresponding to one of the “broken-symmetry” wave function and the high-spin state for complex **3** are described in Figure 7, where α and β spin states are denoted by positive (blue) and negative (green) signs, respectively. The broken-symmetry spin population values at the magnetic centers are +0.57 on Cu(1) and -0.57 on Cu(2) and the spin delocalization is considerable (~43% of the spin is delocalized to the ligand framework). The spin population computed at the pyridine N3/N9 and Cl ligand atoms have the same signs as that of the Cu metal centers to which they are bonded (see Table 2). The spin population on the N3 and N9 atoms is identical in the HS broken-symmetry states of complex **3**, and it is considerably smaller than the values measured at the bridging Cl atoms (0.14 and 0.17 e for Cl1 and Cl3), thus suggesting that chlorido bridging ligands are more effective mediating the magnetic exchange. In fact, the spin population in C4 is negligible, in accordance to fact that the magnetic super-exchange is not mediated through the π -system of

adenine. Plots of the magnetic orbitals are given in the Figure 8 showing the contribution of $d_{x^2-y^2}$ atomic orbitals of the Cu atoms along with the orbitals of the bridging Cl atoms. The $d_{x^2-y^2}$ atomic orbitals of the Cu atoms are not coplanar with the adenine planes; instead, they are out of plane in 21° the Cu1 and 30° the Cu2.

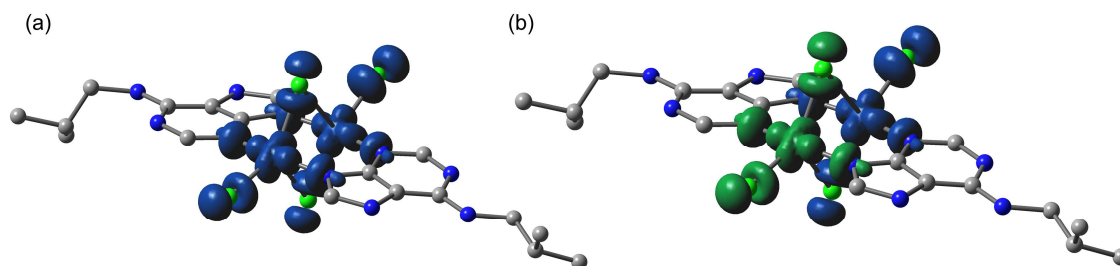


Figure 7. Representation of spin density (contour $0.004 \text{ e } \text{\AA}^{-3}$) at the high spin (a) and low spin (b) configurations of 3. Positive spin represented in blue and negative spin in green.

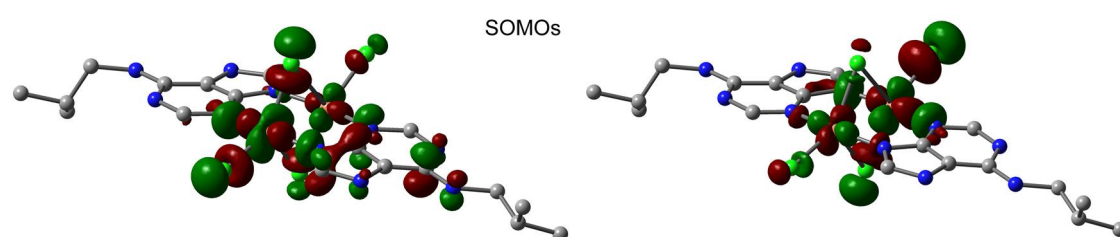


Figure 8. Graphical representation (contour $0.02 \text{ e } \text{\AA}^{-3}$) of the single occupied molecular orbitals (SOMOs) of complex 3.

3. Materials and Methods

3.1. Starting Materials

All the chemicals were of reagent grade and were commercially available. They were used without further purification. The ligands were synthesized using the methodology available in the literature.

3.2. Synthesis of the Complex $[\text{Cu}_2(\mu\text{-HL}^1)_2(\mu\text{-Cl})_2\text{Cl}_2]\text{Cl}_2 \cdot 2\text{H}_2\text{O}$ (1)

A solution (3 mL) of 170 mg (1 mmol) of $\text{CuCl}_2 \cdot 2\text{H}_2\text{O}$ in HCl (2M) was added to a HCl (2 M) solution (2 mL) of HL^1 (0.5 mmol) with stirring. The resulting solution was refluxed for 4 h, filtered and allowed to cool at room temperature. Diffraction quality single crystals (dark green) were obtained after two months.

Yield: 0.073 g (40%). $\text{C}_{16}\text{H}_{28}\text{N}_{10}\text{Cl}_6\text{Cu}_2\text{O}_2$ (727.91 g/mol). Calculated: C, 26.24; H, 3.85; N, 19.13. Found: C, 26.18; H, 3.74; N, 18.91. IR (cm^{-1}): 3440m, 3315m, 3159m, 3093m, 3013s, 2923s br, 1697vs, 1652sh, 1621s, 1579m, 1537m, 1493w, 1467s, 1396s, 1338m, 1300m, 1226s, 1164w, 1129m, 991w, 960w, 802m, 771m, 671m, 659m, 610m, 574m, 557m. EPR: $g_{\text{iso}} = 2.18$.

3.3. Synthesis of the Complex $[\text{Cu}_2(\mu\text{-HL}^2)_2(\mu\text{-Cl})_2\text{Cl}_2]\text{Cl}_2 \cdot 3\text{H}_2\text{O}$ (2)

A solution (3 mL) of 170 mg (1 mmol) of $\text{CuCl}_2 \cdot 2\text{H}_2\text{O}$ in HCl (2M) was added to a HCl (2 M) solution (2 mL) of HL^2 (0.5 mmol) with stirring. The resulting solution was refluxed for 4 h, filtered and allowed to cool at room temperature. Diffraction quality single crystals (dark green) were obtained after two weeks.

Yield: 0.066 g (35%). $\text{C}_{16}\text{H}_{34}\text{N}_{10}\text{Cl}_6\text{Cu}_2\text{O}_3$ (749.95 g/mol). Calculated: C, 27.78; H, 4.40; N, 18.00. Found: C, 27.83; H, 4.35; N, 17.85. IR (cm^{-1}): 3436m, 3313m, 3156m, 2929s br, 2869s, 1697vs, 1657sh,

1625s, 1577m, 1538m, 1467s, 1398s, 1357w, 1297w, 1227s, 1165w, 1126w, 925w, 818m, 773m, 660m, 610m, 574m, 552m. EPR: $g_{\text{iso}} = 2.13$.

3.4. Synthesis of the Complex $[\text{Cu}_2(\mu\text{-HL}^3)_2(\mu\text{-Cl})_2\text{Cl}_2]\text{Cl}_2 \cdot 2\text{H}_2\text{O}$ (2)

A solution (3 mL) of 170 mg (1 mmol) of $\text{CuCl}_2 \cdot 2\text{H}_2\text{O}$ in HCl (2M) was added to a HCl (2 M) solution (2 mL) of HL^3 (0.5 mmol) with stirring. The resulting solution was refluxed for 4 h, filtered and allowed to cool at room temperature. Diffraction quality single crystals (dark green) were obtained after two weeks.

Yield: 0.101 g (55%). $\text{C}_{16}\text{H}_{32}\text{N}_{10}\text{Cl}_6\text{Cu}_2\text{O}_2$ (731.94 g/mol). Calculated: C, 28.43; H, 4.24; N, 18.42. Found: C, 28.44; H, 4.21; N, 18.16. IR (cm^{-1}): 3502m, 3299m, 3157m, 2910s br, 1698vs, 1656sh, 1616s, 1532m, 1467m, 1445m, 1396s, 1334m, 1304m, 1269m, 1226s, 1173m, 1138m, 1112m, 1022w, 971w, 928w, 815s, 773s, 656m, 609s, 498w. EPR: $g_{\text{iso}} = 2.16$.

3.5. Physical Measurements

Elemental analyses (C, H and N) were performed using a Perkin-Elmer 2400 series II CHN analyzer. IR spectra in KBr pellets ($4000\text{--}500\text{ cm}^{-1}$) were recorded using a Perkin-Elmer RXI FT-IR spectrophotometer. The EPR spectra were recorded with an ESP 300 E spectrometer (Bruker, Karlsruhe, Germany), with a frequency of 9.6 GHz. Temperature-dependent molar susceptibility for powdered samples of **1** and **3** were measured with a superconducting quantum interference device vibrating sample magnetometer (SQUID-VSM, Quantum Design) with an applied field of 1 T throughout the temperature range, 2–300 K. The susceptibility data were corrected by Pascal's diamagnetic contributions.

3.6. Computational Methodology

Theoretical calculations based on broken symmetry DFT have been used to estimate the coupling constants (J) of these complexes using the methodology and equation $[E_{\text{BS}} - E_{\text{HS}} = (2S_1 \cdot S_2 + S_2) \cdot J_{12}]$ as proposed by Ruiz et al. [29]. X-ray coordinates were used in these calculations. The hybrid B3LYP functional [30–32] and widely employed 6-31+G* basis set [33] has been considered in the calculations including the Cu(II) ions, as implemented in the Gaussian-09 package [34]. The spin density plots and molecular orbitals have been represented using GaussView 6.0 [34]. We have also used a larger basis set for the calculation (6-311+G**) of the magnetic coupling constants [35,36], however the agreement of the theoretical J values with the experimental ones was slightly worse.

3.7. X-ray Crystallography

Suitable single crystals of complexes **1–3** were selected for X-ray single crystal diffraction experiments and mounted at the tip of glass fibres on an Enraf-Nonius CAD4 diffractometer producing graphite monochromated $\text{MoK}\alpha$ radiation ($\lambda = 0.71073\text{ \AA}$). In each case, after the random search of 25 reflections, the indexation procedure gave rise to the cell parameters (see Table 1 for a summary of the crystal data). Intensity data were collected in the $\omega\text{-}2\theta$ scan mode and corrected for Lorentz and polarization effects. The absorption correction was performed following the empirical DIFABS method [37]. The structural resolution procedure was made using the WinGX package [38]. Solving for structure factor phases was performed by SIR2002 [39] (compound **3**) and SIR2004 [40] (compounds **1** and **2**), and the full matrix refinement by SHELXL-2017/1 [41] for the three crystals. Non-H atoms were refined anisotropically and H-atoms were introduced in calculated positions and refined riding on their parent atoms, except of those belonging to the water molecules, which were located in the difference Fourier maps and refined isotropically. In compound **1**, two of the water molecules (numbered 3 and 4) present partial occupancy of 50% each one. Also in compound **1**, the aliphatic chains of the adenines have been split in different positions to account for the observed disorder. Data collection, structure refinement parameters and crystallographic data for complexes **1–3** are given in Table 3.

Table 3. Selected crystallographic data for compounds 1–3.

Compound	1	2	3
Empirical formula	C ₁₈ H ₃₄ Cl ₆ Cu ₂ N ₁₀ O ₃	C ₁₆ H ₂₈ Cl ₆ Cu ₂ N ₁₀ O ₂	C ₁₈ H ₃₂ Cl ₆ Cu ₂ N ₁₀ O ₂
Formula weight	778.33	732.26	760.31
Temperature (K)	294	294	294
Wavelength (Å)	MoK α	MoK α	MoK α
Crystal system	triclinic	triclinic	monoclinic
Space group	P-1	P-1	P2 ₁ /c
Unit cell dimensions			
a (Å)	9.508(3)	9.529(2)	9.521(3)
b (Å)	13.341(4)	11.482(3)	23.356(8)
c (Å)	14.067(3)	14.226(4)	13.621(9)
α (°)	66.62(3)	67.80(2)	90
β (°)	73.68(2)	75.17(2)	99.35(4)
γ (°)	81.53(2)	88.03(2)	90
Volume (Å ³)	1570.5(8)	1389.7(6)	2989(2)
Z	2	2	4
Density (calculated) (Mg/m ³)	1.646	1.75	1.69
Absorption coefficient (mm ⁻¹)	1.904	2.143	1.996
F(000)	792	740	1544
Crystal size (mm ³)	0.32 × 0.24 × 0.17	0.3 × 0.3 × 0.3	0.46 × 0.28 × 0.13
Theta range for data collection (°)	1.627 to 24.974	1.602 to 24.969	2.168 to 28.445
Index ranges	−10 ≤ h ≤ 11	−10 ≤ h ≤ 11	−12 ≤ h ≤ 12
	−14 ≤ k ≤ 15	−12 ≤ k ≤ 13	−31 ≤ k ≤ 0
	0 ≤ l ≤ 16	0 ≤ l ≤ 16	0 ≤ l ≤ 18
Reflections collected	5520	4872	7507
Independent reflections	5520	4872	7507
Completeness to final theta (%)	100%	99.8%	99.5%
Absorption correction	Empirical (DIFABS)	Empirical (DIFABS)	Empirical (DIFABS)
Max. and min. transmission	0.7235 and 0.4332	0.9385 and 0.5657	0.781 and 0.46
Refinement method		Full-matrix least-squares on F ²	
Data/restraints/parameters	5520/489/506	4872/332/343	7507/6/360
Goodness-of-fit on F ²	0.944	0.896	0.892
Final R indices [I > 2 σ (I)]	R ₁ = 0.0717, wR ₂ = 0.1335	R ₁ = 0.0891, wR ₂ = 0.1469	R ₁ = 0.0489, wR ₂ = 0.1098
R indices (all data)	R ₁ = 0.171, wR ₂ = 0.1609	R ₁ = 0.2495, wR ₂ = 0.1838	R ₁ = 0.2125, wR ₂ = 0.1319
Largest diff. peak and hole (e.Å ⁻³)	0.426 and −0.536	1.032 and −0.72	0.91 and −0.7
CCDC code	1840949	1840950	1840951

4. Conclusions

The synthesis and characterization of three dinuclear copper(II) complexes with N⁶-alkyl bidentate N³,N⁹ donor adeninium bases ligands and chlorido co-ligands are described in this paper. The structures were characterized by X-ray crystal structure and the solid state structures of all three complexes show the participation of the organic ligand in concurrent hydrogen bonding, anion– π interactions involving the six membered aromatic ring and the chloride counter-anions. In the dinuclear copper(II) complexes the two magnetic centers are connected by chlorido ligands atoms, forming a Cu₂Cl₂ core. The magnetic characterization shows the presence of antiferromagnetic Cu–Cu coupling through the chlorido bridges, which has been rationalized using DFT calculations by means of spin density and orbital plots.

Supplementary Materials: The following are available online at <http://www.mdpi.com/2312-7481/4/2/24/s1>, Figure S1: H-bonding network forming 2D supramolecular structures in compound 1, Figure S2: H-bonding network forming 2D supramolecular structures in compound 2, Figure S3: EPR spectra of compounds 1 and 3, Table S1: Coordination distances (Å) and angles (°) for compounds 1–3, Table S2: Geometric features of the hydrogen bonds in compound 1. Distances in Å and angles in degrees, Table S3: Geometric features of the hydrogen bonds in compound 2. Distances in Å and angles in degrees. Table S4: Absolute energies and <S²> values for the HS and LS configurations of compounds 1 and 3.

Author Contributions: Á.G.-R. and A.F. conceived and designed the experiments; M.S.M. performed the synthesis; E.M. and M.B.-O. carried out the X-ray measurements and characterization; A.C. carried out the magnetic measurements. J.J.F. and Á.T. analyzed the data; A.B. performed the theoretical study; A.F. wrote the paper.

Acknowledgments: We thank the Ministerio de Economía y Competitividad (MINECO/AEI) of Spain (projects ENE2015-63969, SEV2015-0496, CTQ2014-57393-C2-1-P, CTQ2017-90802-REDT and CTQ2017-85821-R, FEDER funds) and the Govern de les Illes Balears (Accions Especials de R+D+I with FEDER funds AAEE039/2017) for financial support. We thank the “Centre de Tecnologies de la Informació” (CTI) at the Universitat de les Illes Balears for computational facilities. We thank Francisca Maria Albertí for her participation in the initial synthesis of the compounds.

Conflicts of Interest: The authors declare no conflict of interest.

References

1. Lippert, B. *Progress in Inorganic Chemistry*; Karlin, K.D., Ed.; Wiley: New York, NY, USA, 2005; Volume 54, Chapter 6.
2. Lippert, B. *Nucleic Acid-Metal Ion Interactions*; Hud, N.V., Ed.; RSC Publishing: Cambridge, UK, 2009; Chapter 2.
3. Lippert, B. Multiplicity of metal ion binding patterns to nucleobases. *Coord. Chem. Rev.* **2000**, *200–202*, 487–516. [[CrossRef](#)]
4. Verma, S.; Mishra, A.K.; Kumar, J. The Many Facets of Adenine: Coordination, Crystal Patterns, and Catalysis. *Acc. Chem. Res.* **2010**, *43*, 79–91. [[CrossRef](#)] [[PubMed](#)]
5. Beobide, G.; Castillo, O.; Cepeda, J.; Luque, A.; Perez-Yáñez, S.; Roman, P.; Thomas-Gipson, J. Metal-carboxylato-nucleobase systems: From supramolecular assemblies to 3D porous materials. *Coord. Chem. Rev.* **2013**, *257*, 2716–2736. [[CrossRef](#)]
6. Yang, E.C.; Zhao, H.K.; Feng, Y.; Zhao, X.J. A Tetranuclear Cu^{II}-Based 2D Aggregate with an Unprecedented Tetradentate μ_4 -N1,N3,N7,N9-Adeninate Nucleobase. *Inorg. Chem.* **2009**, *48*, 3511–3513. [[CrossRef](#)] [[PubMed](#)]
7. García-Teran, J.P.; Castillo, O.; Luque, A.; García-Couceiro, U.; Roman, P.; Lloret, F. One-Dimensional Oxalato-Bridged Cu(II), Co(II), and Zn(II) Complexes with Purine and Adenine as Terminal Ligands. *Inorg. Chem.* **2004**, *43*, 5761–5770. [[CrossRef](#)] [[PubMed](#)]
8. Choquesillo-Lazarte, D.; Brandi-Blanco, M.P.; García-Santos, I.; Gonzalez-Perez, J.M.; Castiñeiras, A.; Niclos-Gutierrez, J. Interligand interactions involved in the molecular recognition between copper(II) complexes and adenine or related purines. *Coord. Chem. Rev.* **2008**, *252*, 1241–1256. [[CrossRef](#)]
9. García-Teran, J.P.; Castillo, O.; Luque, A.; García-Couceiro, U.; Beobide, G.; Roman, P. Supramolecular architectures assembled by the interaction of purine nucleobases with metal-oxalato frameworks. Non-covalent stabilization of the 7H-adenine tautomer in the solid-state. *Dalton Trans.* **2006**, *7*, 902–911. [[CrossRef](#)] [[PubMed](#)]
10. Cepeda, J.; Castillo, O.; García-Teran, J.P.; Luque, A.; Perez-Yáñez, S.; Roman, P. Supramolecular Architectures and Magnetic Properties of Self-Assembled Windmill-Like Dinuclear Copper(II) Complexes with Purine Ligands. *Eur. J. Inorg. Chem.* **2009**, *2009*, 2344–2353. [[CrossRef](#)]
11. Suggs, J.W.; Dube, M.J.; Nichols, M. Synthesis and structure of a product, formed during DNA nicking with a cyclometallated nuclease, consisting of an adenine bridging two palladium(II) complexes. *J. Chem. Soc. Chem. Commun.* **1993**, *3*, 307–309. [[CrossRef](#)]
12. Wei, C.H.; Jacobson, K.B. X-ray crystallographic characterization of an adenine-cadmium(II) complex, di- μ -adeninium-di- μ -aquo-tetrakis(nitrato-O,O')dicadmium(II) dinitrate, containing a cationic nucleic acid base as a bidentate ligand. *Inorg. Chem.* **1981**, *20*, 356–363. [[CrossRef](#)]
13. Gagnon, C.; Hubert, J.; Rivest, R.; Beauchamp, A.L. Crystal structure of di- μ -adeninium-disilver(I) perchlorate monohydrate. *Inorg. Chem.* **1977**, *16*, 2469–2473. [[CrossRef](#)]
14. Terzis, A.; Beauchamp, A.L.; Rivest, R. Crystal and molecular structure of diaquotetra- μ -adeninediaquodicopper(I) perchlorate dihydrate, $[\text{Cu}_2(\text{C}_5\text{H}_5\text{N}_5)_4(\text{H}_2\text{O})_2](\text{ClO}_4)^{4+} \cdot 2\text{H}_2\text{O}$. *Inorg. Chem.* **1973**, *12*, 1166–1170. [[CrossRef](#)]
15. De Meester, P.; Skapski, A.C. Crystal structure of dichlorotetra- μ -adenine-dicopper(II) chloride hexahydrate. *J. Chem. Soc. A* **1971**, 2167–2169. [[CrossRef](#)]
16. Mastropietro, T.F.; Armentano, D.; Marino, N.; De Munno, G. Metal-nucleobase interactions in magnesium(II) and manganese(II) complexes with adenine: Influence of the anion on the non-covalent stabilization of 7H-adenine tautomer. *Polyhedron* **2007**, *26*, 4945–4954. [[CrossRef](#)]

17. Gonzalez-Perez, J.M.; Alarcon-Payer, C.; Castiñeiras, A.; Pivetta, T.; Lezama, L.; Choquesillo-Lazarte, D.; Crisponi, G.; Niclós-Gutierrez, J. A Windmill-Shaped Hexacopper(II) Molecule Built Up by Template Core-Controlled Expansion of Diaquatetrakis(μ_2 -adeninato-N3,N9)dicopper(II) with Aqua(oxydiacetato)copper(II). *Inorg. Chem.* **2006**, *45*, 877–882. [[CrossRef](#)] [[PubMed](#)]
18. Perez-Yáñez, S.; Beobide, G.; Castillo, O.; Cepeda, J.; Luque, A.; Roman, P. Directing the Formation of Adenine Coordination Polymers from Tunable Copper(II)/Dicarboxylato/Adenine Paddle-Wheel Building Units. *Cryst. Growth Des.* **2012**, *12*, 3324–3334. [[CrossRef](#)]
19. Thomas-Gipson, J.; Beobide, G.; Castillo, O.; Fröba, M.; Hoffmann, F.; Luque, A.; Pérez-Yáñez, S.; Román, P. Paddle-Wheel Shaped Copper(II)-Adenine Discrete Entities as Supramolecular Building Blocks to Afford Porous Supramolecular Metal-Organic Frameworks (SMOFs). *Cryst. Growth Des.* **2014**, *14*, 4019–4029. [[CrossRef](#)]
20. Reger, D.L.; Pascui, A.E.; Smith, M.D.; Jezierska, J.; Ozarowski, A. Halide and Hydroxide Linearly Bridged Bimetallic Copper(II) Complexes: Trends in Strong Antiferromagnetic Superexchange Interactions. *Inorg. Chem.* **2012**, *51*, 7966–7968. [[CrossRef](#)] [[PubMed](#)]
21. Reger, D.L.; Pascui, A.E.; Smith, M.D.; Jezierska, J.; Ozarowski, A. Syntheses, Structural, Magnetic, and Electron Paramagnetic Resonance Studies of Monobridged Cyanide and Azide Dinuclear Copper(II) Complexes: Antiferromagnetic Superexchange Interactions. *Inorg. Chem.* **2015**, *54*, 1487–1500. [[CrossRef](#)] [[PubMed](#)]
22. Jana, S.; Shaw, B.K.; Bhowmik, P.; Harms, K.; Drew, M.G.B.; Chattopadhyay, S.; Saha, S.K. Field-Induced Ferromagnetism and Multiferroic Behavior in End-on Pseudohalide-Bridged Dinuclear Copper(II) Complexes with Tridentate Schiff Base Blocking Ligands. *Inorg. Chem.* **2014**, *53*, 8723–8734. [[CrossRef](#)] [[PubMed](#)]
23. Thomas-Gipson, J.; Pérez-Aguirre, R.; Beobide, G.; Castillo, O.; Luque, A.; Pérez-Yáñez, S.; Román, P. Unravelling the Growth of Supramolecular Metal-Organic Frameworks Based on Metal-Nucleobase Entities. *Cryst. Growth Des.* **2015**, *15*, 975–983. [[CrossRef](#)]
24. Tsuboi, M.; Takahashi, S.; Harada, I. *Physicochemical Properties of Nucleic Acids*; Duchesne, J., Ed.; Academic Press: London, UK, 1973; Volume 2, pp. 91–145.
25. Pérez-Aguirre, R.; Beobide, G.; Castillo, O.; de Pedro, I.; Pérez-Yáñez, S. Supramolecular extended systems based on discrete paddle-wheel shaped metal-adeninate entities. *Inorg. Chim. Acta* **2016**, *452*, 222–228. [[CrossRef](#)]
26. Fiol, J.J.; Barcelo-Oliver, M.; Tasada, A.; Frontera, A.; Terron, A.; Garcia-Raso, A. Structural characterization, recognition patterns and theoretical calculations of long-chain N-alkyl substituted purine and pyrimidine bases as ligands: On the importance of anion- π interactions. *Coord. Chem. Rev.* **2013**, *257*, 2705–2715. [[CrossRef](#)]
27. Garcia-Raso, A.; Alberti, F.M.; Fiol, J.J.; Lagos, Y.; Torres, M.; Molins, E.; Mata, I.; Estarellas, C.; Frontera, A.; Quinonero, D.; et al. A Combined Experimental and Theoretical Study of Anion- π Interactions in N⁶- and N⁹-Decyladenine Salts. *Eur. J. Org. Chem.* **2010**, *2010*, 5171–5180. [[CrossRef](#)]
28. Garcia-Raso, A.; Alberti, F.M.; Fiol, J.J.; Tasada, A.; Barcelo-Oliver, M.; Molins, E.; Escudero, D.; Frontera, A.; Quinonero, D.; Deya, P.M. Anion- π Interactions in Bisadenine Derivatives: A Combined Crystallographic and Theoretical Study. *Inorg. Chem.* **2007**, *46*, 10724–10735. [[CrossRef](#)] [[PubMed](#)]
29. Ruiz, E.; Rodríguez-Forte, A.; Cano, J.; Alvarez, S.; Alemany, P. About the calculation of exchange coupling constants in polynuclear transition metal complexes. *J. Comput. Chem.* **2013**, *24*, 982–989. [[CrossRef](#)] [[PubMed](#)]
30. Becke, A.D. Density-functional thermochemistry. III. The role of exact exchange. *J. Chem. Phys.* **1993**, *98*, 5648–5652. [[CrossRef](#)]
31. Lee, C.; Yang, W.; Parr, R.G. Development of the Colle-Salvetti correlation-energy formula into a functional of the electron density. *Phys. Rev. B* **1988**, *37*, 785–789. [[CrossRef](#)]
32. Becke, A.D. Density-functional exchange-energy approximation with correct asymptotic behavior. *Phys. Rev. A* **1998**, *38*, 3098–3100. [[CrossRef](#)]
33. Rassolov, V.A.; Ratner, M.A.; Pople, J.A.; Redfern, P.C.; Curtiss, L.A. 6-31G* Basis Set for Third-Row Atoms. *J. Comput. Chem.* **2001**, *22*, 976–984. [[CrossRef](#)]
34. Frisch, M.J.; Trucks, G.W.; Schlegel, H.B.; Scuseria, G.E.; Robb, M.A.; Cheeseman, J.R.; Scalmani, G.; Barone, V.; Mennucci, B.; Petersson, G.A.; et al. *Gaussian 09, Revision D.01*; Gaussian, Inc.: Wallingford, CT, USA, 2009.

35. Baryshnikov, G.V.; Minaev, B.F.; Baryshnikova, A.A.; Ågren, H. Anion-induced exchange interactions in binuclear complexes of Cu(II) with flexible hexadentate bispicolylamidrazone ligands. *Chem. Phys. Lett.* **2016**, *661*, 48–52. [[CrossRef](#)]
36. Baryshnikov, G.V.; Minaev, B.F.; Baryshnikova, A.T.; Ågren, H. A computational study of structural and magnetic properties of bi- and trinuclear Cu(II) complexes with extremely long Cu—Cu distances. *Chem. Phys.* **2017**, *491*, 48–55. [[CrossRef](#)]
37. Walker, N.; Stuart, D. An empirical method for correcting diffractometer data for absorption effects. *Acta Crystallogr. A* **1983**, *39*, 158–166. [[CrossRef](#)]
38. Farrugia, L.J. WinGX suite for small-molecule single-crystal crystallography. *J. Appl. Crystallogr.* **1999**, *32*, 837–838. [[CrossRef](#)]
39. Burla, M.C.; Camalli, M.; Carrozzini, B.; Cascarano, G.L.; Giacovazzo, C.; Polidori, G.; Spagna, R. SIR2002: The program. *J. Appl. Crystallogr.* **2003**, *36*, 1103. [[CrossRef](#)]
40. Burla, M.C.; Caliandro, R.; Camalli, M.; Carrozzini, B.; Cascarano, G.L.; De Caro, L.; Giacovazzo, C.; Polidori, G.; Spagna, R. SIR2004: An improved tool for crystal structure determination and refinement. *J. Appl. Crystallogr.* **2005**, *38*, 381–388. [[CrossRef](#)]
41. Sheldrick, G.M. Crystal structure refinement with SHELXL. *Acta Crystallogr.* **2015**, *71*, 3–8. [[CrossRef](#)]



© 2018 by the authors. Licensee MDPI, Basel, Switzerland. This article is an open access article distributed under the terms and conditions of the Creative Commons Attribution (CC BY) license (<http://creativecommons.org/licenses/by/4.0/>).